Fourier Plane Imaging Microscopy for Detection of Plasmonic Crystals with Periods beyond the Optical Diffraction Limit

Daniel Dominguez, Mdhaoui Alhusain, Nouf Alharbi, Ayrton Bernussi & Luis Grave de Peralta

Plasmonics

ISSN 1557-1955

Plasmonics
DOI 10.1007/s11468-015-9938-x

Springer

Plasmonics
DOI 10.1007/s11468-015-9938-x

Fourier Plane Imaging Microscopy for Detection of Plasmonic Crystals with Periods beyond the Optical Diffraction Limit

Daniel Dominguez[1,2] · **Mdhaoui Alhusain**[1] · **Nouf Alharbi**[1] · **Ayrton Bernussi**[2,3] · **Luis Grave de Peralta**[1,2]

Received: 4 June 2014 / Accepted: 24 March 2015

Abstract Using a simple optical microscope, composed of a plasmonic ultrathin condenser, an objective lens, and a camera, we show that the captured Fourier plane images can provide more information than the real plane images that would be obtained from the corresponding compound microscope. Using this simple Fourier plane imaging approach, we demonstrate that reconstructed non-scanning images of plasmonic crystals with lateral resolution beyond the optical diffraction limit can be obtained.

Keywords Microscopy · Surface plasmons · Image formation theory · Image processing · Resolution

Introduction

The compound microscope is a well-established and thoroughly studied instrument designed for optical imaging of microscopic objects. A typical compound microscope includes an objective lens, in which a Fourier plane (FP) image of the object under observation is formed, and an eyepiece consisting of a second set of lenses designed to transform the FP image in to an image of the object [1–3]. The real plane (RP) image is often collected by a camera in modern compound microscopes and, after some digital processing, is displayed on a computer screen. However, it is well-known that the intrinsic diffraction limit of light prevents diffraction-based imaging instruments from being able to image features with subwavelength dimensions [1–4]. Therefore, modern development challenges focus on creating alternative optical instruments that are as easy-to-use and flexible as the compound microscope, yet capable of addressing the characterization challenges posed by the advanced nanofabrication techniques used in the realization of novel materials and devices.

Optical condensers are the oldest and simplest known optical elements used to obtain images with subwavelength resolution. The discovery of the optical condenser by Abbe in 1873 improved the compound microscope by allowing a reduction in the minimum observable period (p_{min}) in a periodic structure from $p_{min}\sim\lambda/NA_o$ to $p_{min}\sim\lambda/(2NA_o)$ [5, 6], where λ is the wavelength of the illumination source in vacuum, and NA_o is the numerical aperture of the microscope objective lens. This resolution increase is due to the steeply inclined illumination provided by the condenser. The minimum value, $p_{min}=\lambda/(2NA_o)$, is the well-known Rayleigh resolution limit for diffraction-limited optical microscopes [1, 2]. Typical condensers currently used in compound microscopes consist of a combination of bulky lenses (or mirrors) and diaphragms designed to illuminate the sample with a cone of light [7]. However, ultrathin condensers (UTC) occupying a volume three orders of magnitude smaller than bulky condensers [8] and digital condensers with no lenses, mirrors, or moving parts [9–11] have been recently demonstrated. Resolution values several times smaller than the Rayleigh resolution limit have been demonstrated using the Fourier ptychographic microscopy (FPM) technique, which is based on the use of a traditional compound microscope with a planar digital condenser, and the synthetic reconstruction of a FP image with a large effective numerical aperture from numerous low resolution RP images [10].

✉ Daniel Dominguez
daniel.dominguez@ttu.edu

[1] Department of Physics, Texas Tech University, Lubbock, TX 79409, USA

[2] Nano Tech Center, Texas Tech University, Lubbock, TX 79409, USA

[3] Department of Electrical and Computer Engineering, Texas Tech University, Lubbock, TX 79409, USA

Published online: 12 April 2015

In this work, we present a simple microscope arrangement and a novel image reconstruction technique used to observe plasmonic crystals [12, 13] with periods much smaller than those bound by the Rayleigh resolution limit. The microscope instrument described here is simpler than compound microscopes since it does not require an eyepiece lens to form the RP image. A plasmonic UTC with a large numerical aperture ($NA_c>1$) is used to illuminate the plasmonic crystal, and a typical charged coupled device (CCD) camera captures the FP image formed at the back focal plane (BFP) of the objective lens in a single shot. Then, a reconstructed RP image of the plasmonic crystal is generated from features found in the captured FP image. We denote this microscopy technique Fourier plane imaging microscopy (FPIM) because the proposed method only requires the capture of the FP image. Similar to the FPM method, the reconstructed RP images obtained with FPIM technique can image features with dimensions smaller than the Rayleigh resolution limit. However, in contrast to FPM where a RP image is captured by a camera for each light emitting diode (LED) in the planar digital condenser used as the illumination source [10], only a single FP image is needed when using FPIM to reconstruct the high resolution RP image. FPIM is also related with the structured illumination technique [14] where several FP images, obtained by illuminating the sample at different directions with spatially structured light, are modified in order to synthesize, as in FPM, a FP image with a large effective numerical aperture. FPIM resembles traditional lensless X-rays diffraction crystallography where the periodic structure of a crystal can be determined from the recorded diffraction pattern [15]; however, the use of an objective lens in FPIM allows for better control of the optical environment and for light collection with large numerical aperture. Moreover, this technique allows for a direct comparison of the synthetic images created using the FPIM technique with the RP images obtained by the camera of a compound microscope that has an objective lens with the same numerical aperture as the one forming the FPIM. By doing so, we were able to clearly demonstrate a remarkable property of the FPIM technique: the captured FP images contain more information than the RP images obtained by the camera of the corresponding compound microscope.

This paper is organized as follows: In Section "Description of the Experiments," we describe the experimental set-up, and the samples used in our experiments. We also describe experimental results constituting a proof-of-principle of the FPIM technique. Section "Discussion of the Experimental Results" is dedicated to the discussion of the experimental results. In Section "Analysis of FP Image Formation," using the image formation theory in microscopes that incorporate UTCs [16], we describe and justify the method used for synthesizing RP images with a resolution more than two times smaller than the Rayleigh resolution limit. Finally, the conclusions of this work are given in Section "Analysis of FP Image Formation".

Description of the Experiments

A schematic illustration of the plasmonic crystal sample's cross-section and the experimental set-up used in our experiments are shown in Fig. 1. The plasmonic crystal, shown in Fig. 1a, is comprised of a ~150-μm glass substrate that is covered with a 45-nm-thick gold layer and coated with a ~110-nm-thick layer of poly-methyl-methacrylate doped with Rhodamine-6G (PMMA-R6G). A 2-nm-thick Cr layer was included in between the glass substrate and gold layer for adhesion purposes.

A periodic array of holes arranged in square and hexagonal lattices, both having period $p=350$ nm and hole diameters $d=p/2$, were patterned by electron-beam lithography in the PMMA-R6G layer. A methyl-isobutyl-keytone:isopranol (MIBK:IPA) 1:3 solution was used to develop the resist exposed by the e-beam leaving air holes in the PMMA-R6G layer. The fluorescent R6G has center-band emission at 568 nm. The samples were exited with a fiber-coupled, continuous-wave, 532-nm wavelength solid state laser, and the omni-directional emitted fluorescence served as the surface plasmon polariton (SPP) excitation source. The experimental arrangement used, shown schematically in Fig. 1b and thoroughly described in [17], consisted of a Nikon Eclipse Ti inverted microscope that was fitted with two charge coupled device (CCD) cameras to acquire RP and FP images. A high numerical aperture ($NA_o=1.49$) ×100 magnification, oil-immersion objective lens, and two low numerical aperture ($NA_o=0.9$ and $NA_o=0.25$) air objectives, having ×100 and ×10 magnification, respectively, were used. The $\lambda=532$ nm laser source was used to illuminate the sample from the top via a NA=0.65 focusing objective. The laser excites the Rhodamine in the doped PMMA layer which in turn excites SPPs at the gold/PMMA interface. Light coupled to SPPs then leaks toward the glass substrate which sits above an objective lens. A $\lambda_o=570$-nm wavelength band-pass filter with a bandwidth of $\Delta\lambda=10$ nm was placed after the objective lens to spectrally filter the leaked and transmitted radiation such that only the light originating from the fluorescence was detected. The CCD cameras were then used to collect FP and RP images corresponding to SPP leakage radiation. It is worth noting that the described plasmonic crystal can be considered a plasmonic UTC [8] where the array or air holes are the object under observation. The combination of the UTC, the objective lens, and the FP CCD camera form the FPIM. In a stand-alone application, the FP camera would be placed in the BFP of the objective lens.

Images of the plasmonic crystals, shown in Fig. 2, were obtained with the ×100 $NA_o=1.49$ oil-immersion objective lens to show that structures were fabricated correctly and that they can be resolved using a sufficiently high NA objective lens. The FP and RP images corresponding to the plasmonic crystal that has the hexagonal lattice with period $p=350$ nm

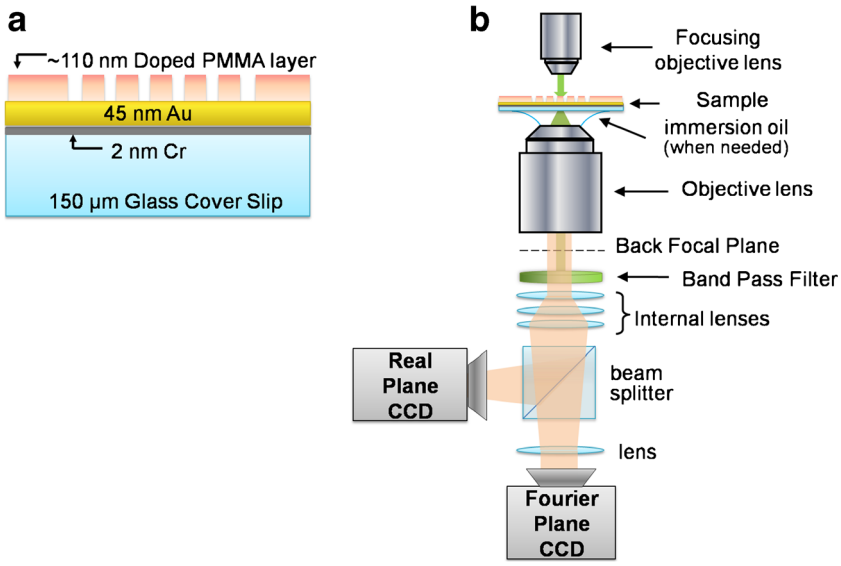

Fig. 1 **a** Cross-section illustration of the plasmonic crystal samples used in our experiments. **b** A schematic representation of the experimental arrangement. The immersion oil is only present when an objective lens with $NA_o = 1.49$ was used

are shown in Fig. 2a, b, respectively, and the FP and RP images corresponding to the square lattice are shown in Fig. 2c, d, respectively. Both FP images revealed three centered concentric rings, where the middle one is the SPP mode corresponding to TM propagation as well as the condenser feature responsible for the increased resolution ability of the UTC [8], while the other two correspond to TE propagation modes [18]. The appearance of the extra rings is indicative of a thick PMMA layer used in our samples [18]. Additional displaced rings were observed in the FP images of these samples whose symmetry is akin to the structure of the lattice in the real plane. The central ring and the displaced rings are reminiscent of diffraction features by hexagonal and square lattices. Therefore, we denoted the central ring as the zero-order diffraction ring and the displaced rings, in analogy, as the first-order diffraction rings. The dim-lit disk-like boundary corresponds to the numerical aperture of the objective lens NA_o. The ratio of the diameter of the zero-order diffraction ring to the diameter of the disk is equal to the ratio of the effective index n_{eff} of the propagating SPP mode to the NA of the collecting microscope objective, that is $n_{eff} = NA_o \cdot r_{SPP}/r_{max}$, where r_{SPP} and r_{max} are the radii of the diffraction rings and the disk-like boundary in the FP images, respectively [17]. By this approach, we determined $n_{eff} = 1.09$ for both the zero-order and the first-order diffraction rings in Fig. 2a, c.

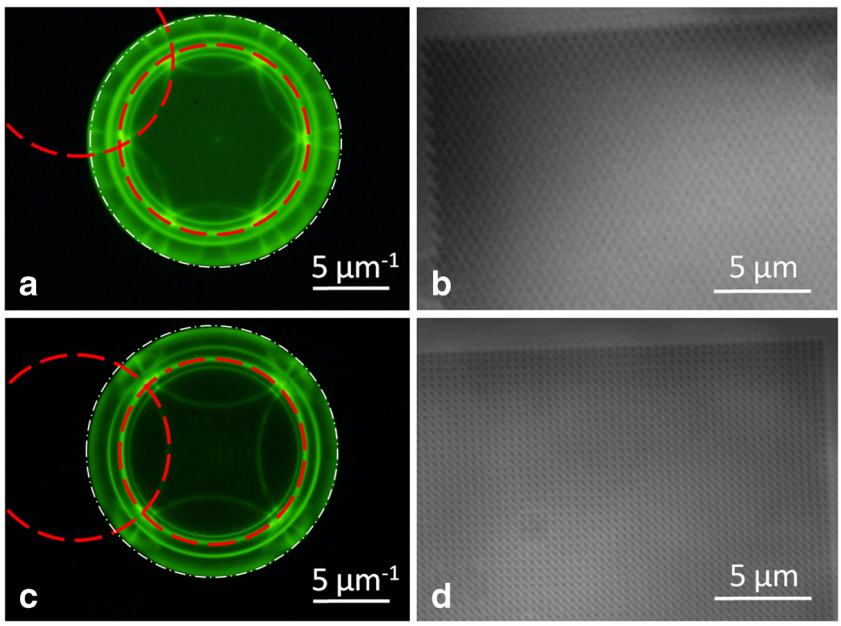

Fig. 2 **a**, **c** FP and **b**, **d** RP images, obtained with a ×100 $NA_o = 1.49$ objective lens, of a plasmonic crystal with $p = 350$ nm having (**a**–**b**) a hexagonal and (**c**–**d**) square lattice geometry. The objective lens' numerical aperture (*white, dash-dot*), the zero-order diffraction ring, and one of the first-order diffraction rings (*red, dashed*) are highlighted

This corresponds to a plasmonic UTC with numerical aperture $NA_c = n_{eff} = 1.09$ [8].

We then replaced the high numerical aperture oil objective lens with a ×100 $NA_o = 0.9$ objective lens and re-imaged the same plasmonic crystal samples shown in Fig. 2. The RP and FP images are shown in Fig. 3. In this arrangement, the FP images (Fig. 3a, c) no longer feature the zero-order diffraction ring but still show portions of the first-order diffraction rings, and the RP images (Fig. 3b, d) no longer show the resolved lattices. The system's inability to image the zero-order diffraction ring is due to the fact that the zero-order ring's numerical aperture is greater than the objective lens' numerical aperture: $NA_c = n_{eff} > NA_o$. Although invisible in the RP image, the plasmonic crystal structure's influence on excited SPPs is evident in the FP image thereby suggesting that more information about the plasmonic crystal's structure can be extracted from the FP images than from the corresponding RP images.

Discussion of the Experimental Results

It has been previously demonstrated [5, 8, 11, 19] that the resolution limit of a compound microscope imaging a periodic sample with a condenser is

$$p_{min} = \frac{\lambda_o}{NA_o + NA_c} \quad (1)$$

Using $\lambda_o = 568$ nm (the SPP exCitation wavelength from the peak fluorescence emission) and $NA_c = n_{eff} = 1.09$, it is no surprise that both the hexagonal and square lattices were resolved using a $NA_o = 1.49$ objective lens (Fig. 2b, d), since the minimum observable period is calculated to be $p_{min} = 220$ nm. For the situation in which $NA_c > NA_o$, expression (1) converges to the limiting p_{min} value defined by $p_{min} = \lambda_o / 2NA_o$ [5] which is the Rayleigh resolution limit. Therefore, when using a $NA_o = 0.9$ objective lens, the Rayleigh criterion determines that the minimum resolvable period should be $p_{min} \sim 315$ nm; however, our results, (Fig. 3b, d), show that this is not the case. This apparent discrepancy can be explained by considering how images in the RP are produced from the FP features. Both the FP and RP images are formed by leakage radiation from a plasmonic UTC. In order to observe a periodic intensity distribution in the RP, features corresponding to at least two diffraction orders must be captured in the FP. In our arrangement, the diffraction features are rings formed from the multidirectional SPP-coupled leakage radiation; as such, portions of (or entire) rings corresponding to two diffraction orders must be captured [19]. The RP images shown in Fig. 3c, d do not contain any information about the plasmonic crystal structure because only portions of the first-order SPP-coupled leakage radiation diffraction rings (and not the zero-order) are collected. A comparison of Figs. 2 and 3 reveals that observation of the plasmonic crystal's periodic structure in the RP image is necessarily contingent on the observation of the zero-order diffraction ring in the FP image. In other words, it is compulsory that $NA_c \leq NA_o$ for compound microscopes that utilize condensers since they are diffraction limited when $NA_c = NA_o$. If it were possible to image plasmonic crystals when $NA_c > NA_o$, then it would be possible to obtain resolution values smaller than the diffraction limit. Such can be accomplished by FPIM as described in what follows:

Figure 4 illustrates part of the procedure used to obtain high-resolution reconstructed images of a plasmonic crystal

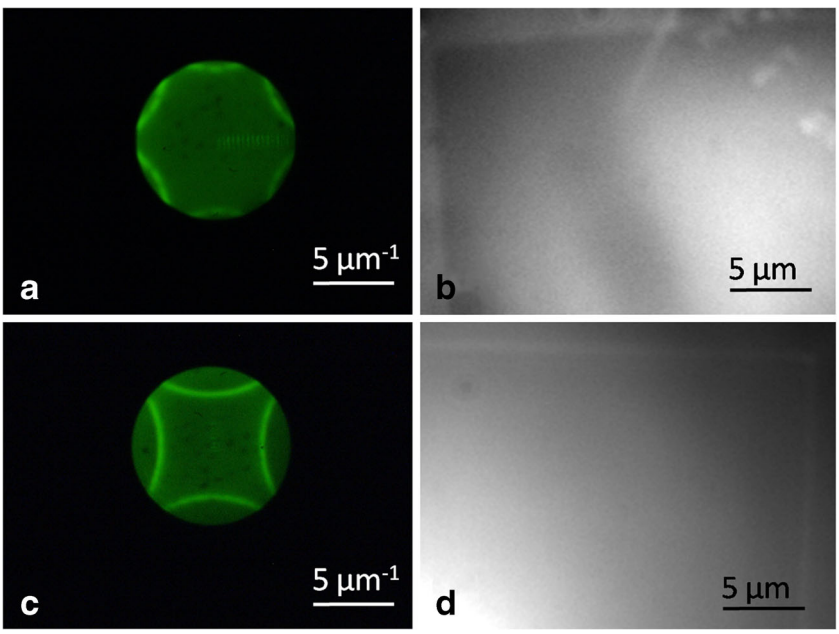

Fig. 3 **a**, **c** FP and **b**, **d** RP images, obtained with a ×100 $NA_o = 0.9$ objective lens, of a plasmonic crystal with $p = 350$ nm having (**a**–**b**) a hexagonal and (**c**–**d**) square lattice geometry

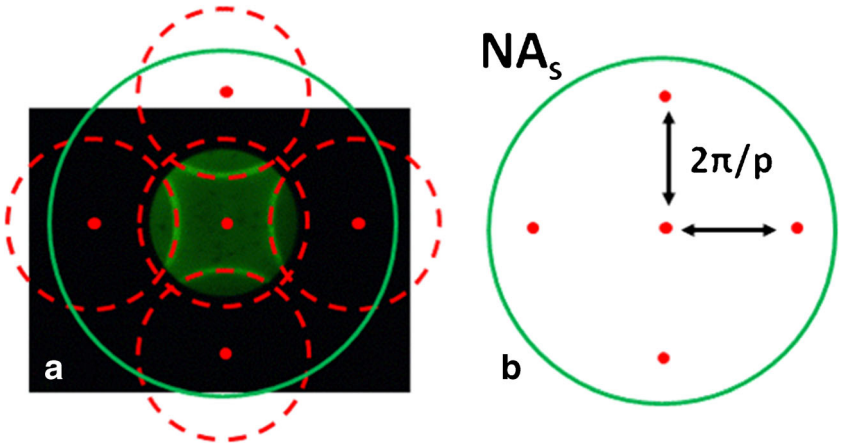

Fig. 4 **a** Picture demonstrating how the synthetic FP image is obtained by generating rings (*dashed red lines*) based on the observed arcs in the numerical aperture and determining their centers (*red dots*). **b** Schematic showing the ring centers and the synthetic numerical aperture NA_s that will be used to produce a reconstructed RP image

with p=350 nm. The FP image seen in Fig. 4a was shown previously in Fig. 3c. To recap, this FP image was obtained using the plasmonic UTC-compound microscope arrangement sketched in Fig. 1 with $NA_c \sim 1.09 > NA_o = 0.9$; therefore, as it is shown in Fig. 3d, the plasmonic crystal features were invisible. Nevertheless, a synthetic FP image with a numerical aperture $NA_s > NA_c$ can be constructed such that spots corresponding to the centers of the first-order diffraction rings, which will be used to generate a reconstructed RP image, can be encompassed by NA_s. This can be realized by generating full first-order diffraction rings based on the portions visible in the FP image, represented by discontinuous lines in Fig. 4a, and determining their respective centers, illustrated by the red dots in Fig. 4a. The zero-order diffraction ring and its center can also easily be generated since the zero-order diffraction ring is centered at the origin of the reciprocal space, and has the same radius as the reconstructed first-order diffraction rings.

Figure 4b shows a simple reconstructed RP image formed by a periodic array of spots with a period $\Lambda = 2\pi/p$ [12, 13, 16] determined from the construction illustrated in Fig. 4a. This simplified synthetic FP image would be formed in the FP camera of the compound microscope if $NA_o = NA_s$ and if the plasmonic crystal were illuminated by a beam of light impinging perpendicularly on the sample. In a first approximation, the five bright spots forming the simplified synthetic FP image shown in Fig. 4b can be described by the optical disturbance $U_{FP,s}$ at the back focal plane of the microscope's objective lens [3, 16]:

$$U_{FP,s}(k_x,k_y) \propto \left[4\delta(k_x,k_y) + \delta\left(k_x - \frac{2\pi}{p},k_y\right) + \delta\left(k_x + \frac{2\pi}{p},k_y\right) + \delta\left(k_x,k_y - \frac{2\pi}{p}\right) + \delta\left(k_x,k_y + \frac{2\pi}{p}\right)\right] \quad (2)$$

where δ is the delta of Dirac function [3], and we have assumed for convenience that the amplitude corresponding to the zero-order diffraction spot four times larger than the amplitude of the first-order diffraction spots. The optical disturbance in the microscope's RP image, $U_{RP,s}(x,y)$, is then proportional to the absolute value of the Fourier transform of $U_{FP}(k_x,k_y)$ [3, 16]; therefore:

$$U_{RP,s}(x,y) \propto \left[2 + \cos\left(\frac{2\pi}{p}x\right) + \cos\left(\frac{2\pi}{p}y\right)\right] \quad (3)$$

Consequently, the two-dimensional periodicity corresponding to the plasmonic crystal can be observed in a reconstructed RP image. This analysis demonstrates that the FP images obtained using a plasmonic UTC-compound microscope arrangement contain more information about the plasmonic crystal's structure than the RP images. As a consequence, FPIM can be used to image plasmonic crystals having a period much smaller than the Rayleigh resolution limit of diffraction-limited optical microscopes. This is illustrated in Fig. 5.

The FP image of a plasmonic crystal with square symmetry and p=550 nm is shown in Fig. 5a. This FP image was obtained using the plasmonic UTC-compound microscope arrangement sketched in Fig. 1 with a ×10 NA_o=0.25 objective lens. Consequently, we estimated the Rayleigh resolution limit for this instrument configuration to be ~1.1 μm. As expected, it was impossible to resolve (not shown) any features of the plasmonic crystal in the RP image obtained with the compound microscope.

Nevertheless, fractions of the four first-order diffraction rings are clearly observed in the FP image shown in Fig. 5a. As it is shown in Fig. 5b, we constructed a synthetic FP image with $NA_s >> NA_o$ and determined a reciprocal space

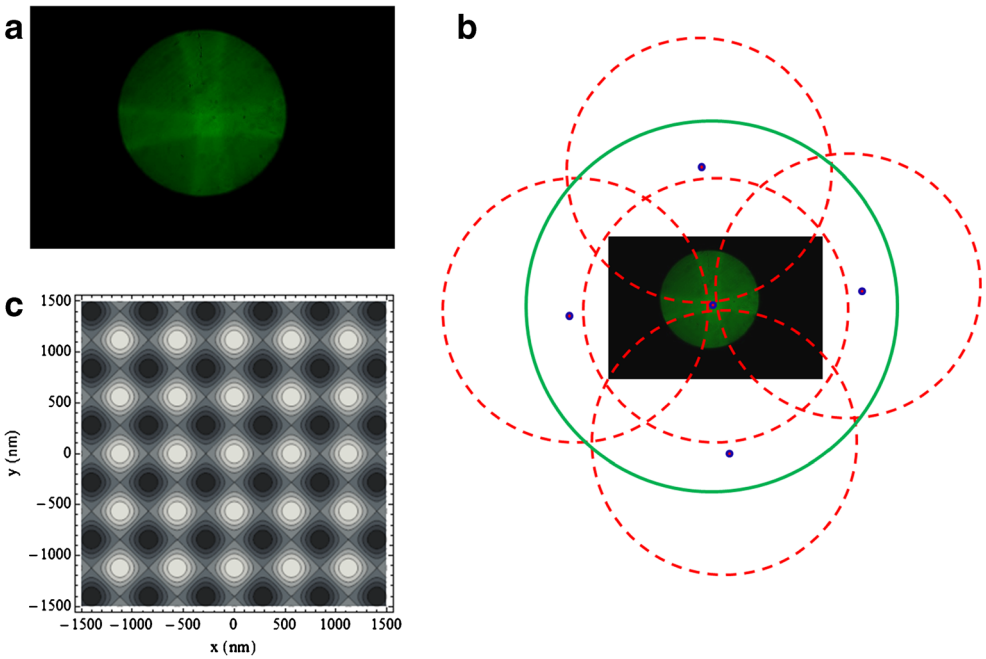

Fig. 5 **a** FP image of plasmonic crystal with a square lattice symmetry and p=550 nm that was taken using a ×10 NA_o=0.25 objective lens. **b** Diagram of the construction of the synthetic FP image, where the *green-solid ring* is the synthetic NA_s, the *red-dashed rings* are the diffraction rings, and the *blue spots* are the ring centers. **c** The reconstructed RP image constructed using Eq. 3 and the value of p obtained from the synthetic FP analysis

separation between spots of Λ=11.2 μm^{-1}. The first-order diffraction rings and the synthetic numerical aperture were included for clarification; however, only the spots are needed for the computational reconstruction of the RP image. In excellent correspondence with the sample fabrication dimensions, we calculated $p=2\pi/\Lambda$=561 nm. Figure 6c shows the reconstructed RP image of the plasmonic crystal using Eq. 3 and the calculated value of p. The image clearly reveals the square lattice symmetry and period of the fabricated plasmonic crystal. This represents a resolution improvement of over two times than that predicted by the Rayleigh resolution criteria of the compound microscope used in this experiment. It is worth noting that this is not the best resolution obtainable with the FPIM technique. By improving the resolution of a microscope that uses a low NA_o objective lens, we can combine the benefits of a large field of view with super-resolution.

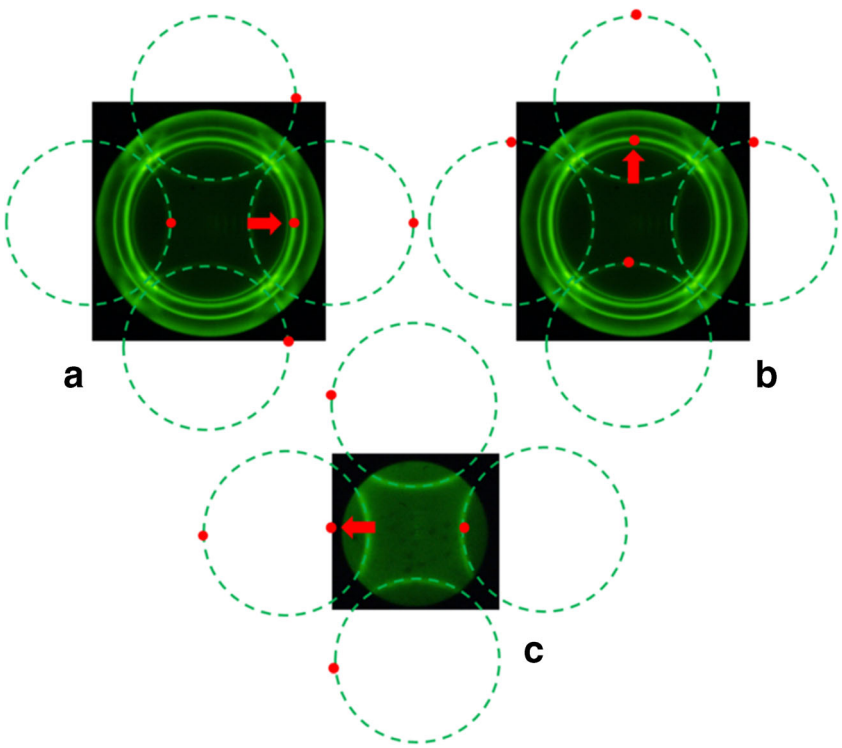

Fig. 6 Schematic illustration of the formation of the FP images shown in (**a**–**b**) Fig. 2c and (**c**) Fig. 3c. The *spots* represent the FP image that would be obtained if the plasmonic crystal were illuminated with a collimated beam of light in the direction indicated by the arrow

Therefore, similar to FPM, FPIM provides an increase in the information content of the RP images [10]. However, FPM requires that multiple RP images be obtained with a compound microscope, while the FPIM technique described in this work has the advantage of only requiring a single-shot image collected at the back focal plane of an objective lens. As it is illustrated by the RP image shown in Fig. 3d, the set of lenses forming the eyepiece of the compound microscope failed to extract the information about the plasmonic crystal's structure contained in the FP image shown in Figs. 3c and 4a. This is because the compound microscope's eyepiece lens is limited to only produce the Fourier transform of the RP image formed in the back focal plane of the microscope's objective lens [3, 16]. However, as we have discussed above, in order to obtain a reconstructed RP image showing the periodicity of the plasmonic crystal, it is necessary to generate the synthetic FP image shown in Fig. 4b, before performing the Fourier transform operation, from the information contained in the FP image shown in Fig. 4a. While the eyepiece failed to image the plasmonic crystal, we succeeded in producing an image of the plasmonic crystal with a period having a value much smaller than the diffraction limit of the light used.

Analysis of FP Image Formation

The set of rings observed in the FP images shown in Figs. 2, 3, 4, and 5 are diffraction rings forming a diffraction pattern; therefore, the formation of the observed rings involves the occurrence of coherent interference of the SPP-coupled leakage radiation used for imaging the plasmonic crystals [16, 20]. As it was previously established [16, 20], in our experiments, SPPs were excited by spontaneous emission fluorescence events, and all the SPP-coupled radiation that leaks in the same direction is coherent. This is because the propagation length of the excited SPPs in the plasmonic crystal is shorter than the coherence length of the fluorescence. However, light leaking in a particular direction from a plasmonic UTC is not coherent with light leaking in another direction [16]. As a consequence, the intensity distribution in the RP images obtained using plasmonic UTCs is given by the incoherent superposition of numerous RP "snap-shots" of leakage radiation in different directions [16]. The observation of a periodic intensity distribution in a RP image, using a plasmonic UTC-compound microscope arrangement, can be analogously characterized as the illumination of, independent, multidirectional, collimated illumination sources.

Figure 6 shows schematic illustrations detailing how the arcs observed in the FP images shown in Fig. 2c (Fig. 6a, c) and Fig. 3c (Fig. 6c) were formed.

The five red spots added to each FP image in Fig. 6 correspond to the diffraction pattern that would be formed at the BFP if the plasmonic crystal were illuminated in a single direction by a coherent light beam incident to the sample at an angle equal to the SPP-coupled leakage radiation angle [16]. The illumination direction is indicated by the arrows, which point to the zero-order diffraction spot. When the direction of illumination rotates, the zero-order diffraction spot traces a circle corresponding to the observed zero-order SPP diffraction ring, while the four first-order diffraction spots produce the observed arcs. As it is illustrated in Fig. 6a, if the plasmonic crystal were illuminated by a collimated beam of light in the "horizontal" direction indicated by the arrow, the zero-order diffraction spot and only one of the four first-order diffraction spots would be captured by the FP camera. Nevertheless, this would be enough to produce a vertically periodic distribution of intensities in the RP image [21]. A similar situation is illustrated in Fig. 6b: if the plasmonic crystal were illuminated by a collimated beam of light in the "vertical" direction indicated by the arrow, the zero-order diffraction spot and only one of the four first-order diffraction spots would also be captured by the FP camera. This would be enough to produce a horizontally periodic distribution of intensities in the RP image [22]. The incoherent superposition of both RP images produces a resultant RP image with square symmetry in good correspondence with the RP image shown in Fig. 2d. This is in contrast with the uniform intensity distribution observed in the RP image shown in Fig. 3d. The FP and RP images shown in Fig. 2c, d, respectively, were obtained with $NA_c > NA_o$. This explains why the FP camera was not able to capture the bright zero-order diffraction ring, which cannot be observed in the FP image shown in Fig. 6c. As it is illustrated by the five red spots added to the FP image shown in Fig. 6c, if the plasmonic crystal were illuminated in any single direction while $NA_c > NA_o$, neither the zero-order diffraction spot nor three of the four first-order diffraction spots would be captured by the FP camera, i.e., only one first-order diffraction spot would be collected by the objective lens of the compound microscope. The RP image shown in Fig. 3d does not contain any information about the plasmonic crystal structure because, as it is illustrated in Fig. 6c, only one first-order diffraction spot is collected. In addition, the Fourier transform of a spot is a broad uniform function [3]; as such, the incoherent superposition of many featureless RP images results in a RP image with no information about the plasmonic crystal. Nevertheless, as it was illustrated in Figs. 4 and 5, the presence of bright arcs in the FP images permits for detection of otherwise invisible-to-the-microscope plasmonic crystals by image reconstruction techniques. It should be noted that this report is meant to demonstrate proof-of-concept of the simplest image reconstruction strategy possible, which is based on the use of Eq. 3 and the simple synthetic FP image shown in Fig. 4b. For instance, numerical calculation of the Fourier transform of the finer details in the FP images shown in Figs. 5b and 6 would reveal additional features of the plasmonic crystal in the reconstructed RP image. Certainly, more

elaborate image reconstruction techniques will be needed for the observation of non-periodic defects in plasmonic crystals.

Conclusions

We have unambiguously shown that the FPIM technique can provide more information about a plasmonic crystal's structure and dimensions from an FP image than that obtained from an RP image obtained with the corresponding compound microscope. By generating a synthetic FP image from the features present in the actual FP image, we were able to reconstruct the RP image of a plasmonic crystal whose periodic structure was half of the Rayleigh limit for the objective lens used. We showed that the FPIM method is a non-scanning technique capable of characterization with minimal image processing plasmonic crystals with sub-wavelength periods.

Acknowledgments This work was partially supported by the NSF CAREER Award (ECCS-0954490).

References

1. Hetcht E (1998) Optics, Thirdth edn. Addison Wesley, Reading
2. Born M, Wolf E (1975) *Principles* of *Optics*, Vth edn. Pergamon Press, Oxford
3. Goodman JW (1968) Introduction to Fourier optics. McGraw-Hill, New York
4. Durant S, Liu Z, Steele JM, Zhang X (2006) Theory of the transmission properties of an optical far-field superlens for imaging beyond the diffraction limit. J Opt Soc Am B 23(11):2383–2392
5. Hopkins HH, Barham PM (1950) The influence of the condenser on microscopic resolution. Proc Phys Soc 63:737–744
6. Köheler H (1981) On Abbe's theory of image formation in the microscope. Opt Acta 28:1691–1701
7. Vainrub A, Pustovyy O, Vodyanoy V (2006) Resolution of 90 nm ($\lambda/5$) in an optical transmission microscope with annular condenser. Opt Lett 31:2855–2857
8. Desai DB, Dominguez D, Bernussi AA, Grave de Peralta L (2014) Ultra-thin condensers for optical subwavelength resolution microscopy. J Appl Phys 115:093103
9. Zheng G, Kolner C, Yang C (2011) Microscopy refocusing and dark-field imaging by using a simple LED array. Opt Lett 36:3987
10. Zheng G, Horstmeyer R, Yang C (2013) Wide-field, high-resolution Fourier ptychographic microscopy. Nat Photonics 7: 739–745
11. Molina L, Dominguez D, Desai DB, O'Loughlin T, Bernussi AA, Grave de Peralta L (2014) Hemispherical digital optical condensers with no lenses, mirrors, or moving parts. Opt Express 22:6948–6957
12. Rodriguez R, Regan CJ, Ruiz-Columbié A, Agutu W, Bernussi AA, Grave de Peralta L (2011) Study of plasmonic crystals using Fourier-plane images obtained with plasmon tomography far-field superlenses. J Appl Phys 110:083109
13. Regan CJ, Grave de Peralta L, Bernussi AA (2012) Equifrequency curve dispersion in dielectric-loaded plasmonic crystals. J Appl Phys 111:073105
14. Gustafsson MG (2000) Surpassing the lateral resolution limit by a factor of two using structured illumination microscopy. J Microsc 198:82–87
15. Kittel C (1996) Introduction to solid state physics, 7th edn. John Wiley & Sons, New York
16. Lopez-Boada R, Regan CJ, Dominguez D, Bernussi AA, Grave de Peralta L (2013) Fundaments of optical far-field subwavelength resolution based on illumination with surface waves. Opt Express 21:11928–11942
17. Frisbie SP, Chesnutt CF, Holtz ME, Krishnan A, Grave de Peralta L, Bernussi AA (2009) Image formation in wide-field microscopes based on leakage of surface plasmon-coupled fluorescence. IEEE Photonics J 1:153
18. Frisbie SP, Regan CJ, Krishnan A, Chesnutt C, Ajimo J, Bernussi AA, Grave de Peralta L (2010) Characterization of polarization states of surface plasmon polariton modes by Fourier-plane leakage microscopy. Opt Commun 283:5255–5260
19. Martin LC (1966) The theory of the microscope. American Elsevier, New York
20. Dominguez D, Regan CJ, Lopez-Boada R, Bernussi AA, Grave de Peralta L (2014) Observation of coherence-related phenomena in experiments with surface plasmon polaritons excited by fluorescence. Opt Commun 315:270–274
21. Regan CJ, Thiabgoh O, Grave de Peralta L, Bernussi AA (2012) Probing photonic Bloch wavefunctions with plasmon-coupled leakage radiation. Opt Express 20:8658
22. Grave de Peralta L, Regan CJ, Bernussi AA (2013) SPP tomography: a simple wide-field nanoscope. Scanning 35:246–252